# Indoor Occupancy Estimation Using Particle Filter and SLEEPIR Sensor System

Muhammad Emad-ud-Din, Zhangjie Chen, Libo Wu, Qijie Shen, and Ya Wang, *Member, IEEE*

***Abstract*—We recently developed a synchronized low energy electronically chopped passive infrared (SLEEPIR) sensor that can detect both stationary and moving occupants by incorporating a liquid crystal (LC) shutter with a traditional passive infrared (PIR) sensor. However, its detection accuracy is still largely impacted by environmental infrared noises. In this paper, we present a Particle Filter (PF) based system-level algorithm that employs a network of SLEEPIR sensors which are installed at different points of interest within an indoor space. The method interprets the incoming observations from the field of view (FOV) of each sensor via the likelihood function to update the state of the PF. The PF output is a probability density function (pdf) that represents the occupancy state of the entire observed space. The sensor location, observation cone, range, observation frequency and historic inter-sensor correlation are the key parameters that contribute to the likelihood function design. Since the method utilizes the historic correlation among sensors, the pairs of correlating sensors often perform self-correction whenever a faulty observation is encountered due to either sensor limitations or due to environmental noise. Occupancy is established through a thresholding function applied to the output pdf of the PF. A lab-based dataset was collected over a period of 360 hours using the SLEEPIR sensor system. Results indicate an average 8.25% occupancy accuracy improvement when compared to the accuracy state delivered by individual SLEEPIR nodes.**

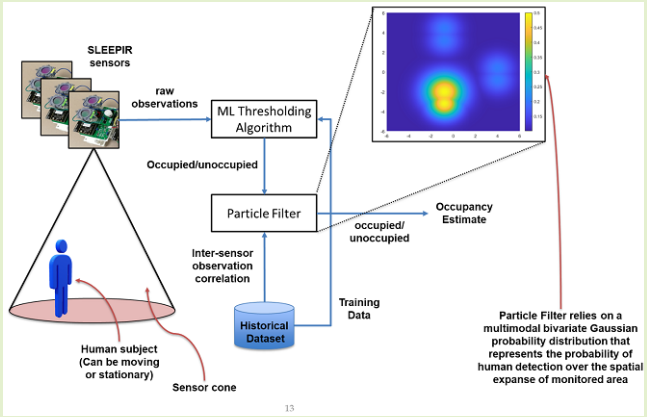


***Index Terms*—Bayes filters, smart devices, recurrent neural networks, edge computing, passive infrared sensors.**

## I. Introduction

THE proposed method is essentially a proof of concept that with limited number of sensors and sparse spatial coverage, a Particle Filter (PF) can be used to track the human occupancy of an indoor space regardless of environmental infrared noises. The method exploits the temporal bounds on the change in occupancy state of the environment. It also factors-in the proximity of sensor nodes to each other, and thus PF measurement updates are structured in a way that human occupancy probability is spread spatially in expanded vicinity around the sensor rather than only inside the sensor observation cone. Human occupancy detection is an essential component of many applications like indoor security systems, lightening and Heating, Ventilation & Airconditioning (HVAC) automation systems, activity tracking systems [1]–[3], and monitoring systems for elderly people who need around the clock care [4]–[6]. Alternate options like camera-based occupancy tracking generally fail to deliver because high infrastructure and computational cost, privacy concerns and failure to track high velocity motions. Apart from cameras, sensors like thermopile arrays [7], IMUs or Wi-Fi sensors are either too noisy or expensive to be part of a scalable solution.

Since passive infrared sensors (PIR) are relatively inexpensive and have been traditionally used in human presence monitoring systems, many have jumped on the opportunity and designed efficient and scalable localization systems based on such sensors. The systems employing such sensors can detect

Manuscript received 21 May 2022; revised 6 July 2022; accepted 8 July 2022. Date of publication 25 July 2022; date of current version 1 September 2022. This work was supported by the U.S. Department of Energy, Advanced Research Projects Agency-Energy (ARPA-E), under Grant DE-AR0000945. The associate editor coordinating the review of this article and approving it for publication was Dr. Yulong Huang. *(Corresponding author: Ya Wang.)*

This work involved human subjects or animals in its research. Approval of all ethical and experimental procedures and protocols was granted by the Institutional Review Board under Application IRB2018-1681D.

Muhammad Emad-ud-Din is with the Department of Computer Science, Texas A&M University, College Station, TX 77843 USA (e-mail: emaad22@tamu.edu).

Zhangjie Chen and Libo Wu are with the J. Mike Walker '66 Department of Mechanical Engineering, Texas A&M University, College Station, TX 77843 USA.

Qijie Shen is with the Department of Electrical and Computer Engineering, Texas A&M University, College Station, TX 77843 USA.

Ya Wang is with the J. Mike Walker '66 Department of Mechanical Engineering, the Department of Electrical and Computer Engineering, and the Department of Biomedical Engineering, Texas A&M University, College Station, TX 77843 USA (e-mail: ya.wang@tamu.edu).

Digital Object Identifier 10.1109/JSEN.2022.3192270

heat energy emitted by human body within a range of roughly 10 meters. However, their incapability of detecting stationary occupants limits their applications in occupancy-centered smart home appliances [8], [9]. To enable PIR sensors to detect stationary occupants, we recently developed a synchronized low energy electronically chopped PIR (SLEEPIR) sensor [10], [11]. The node consists of a PIR sensor, a liquid crystal (LC) infrared shutter and a driving circuit. By electrically chopping the long-wave infrared (8-12$\mu$m) radiation received by the PIR sensor, the SLEEPIR sensor can detection both stationary and moving occupants. However, its detection accuracy is still largely impacted by environmental infrared noises [12], [13].

To address this, we present a PF based human presence estimation algorithm for the SLEEPIR sensor system that includes three sensor nodes sparsely located in an indoor space. The proposed algorithm consumes low-power and is cost-effective and thus provides scalable service which makes the proposed SLEEPIR sensor system eligible for widespread future adoption.

The proposed particle filtering approach involves a PF which relies on three assumptions (1) Any human subjects entering the observed area will trigger at least one SLEEPIR sensor node. (2) The SLEEPIR sensors have a limited Field-of-view (FOV) and thus these only have sparse coverage of the area monitored for human occupancy (3) Collected ground truth data represents the expected traffic conditions within the entire monitored area.

We observed the ground truth data that spanned over 15 days. Although the experiment testbed was artificially created in a lab for dataset collection purposes, yet the experiments were uncontrolled. We installed three SLEEPIR sensor nodes in two different configurations at the testbed to collect dataset as shown in Figure 1. Primary aim of this study is not to optimally cover the testbed space using SLEEPIR sensors but to determine the minimal number of sensors to achieve a level of accuracy that ensures less than 5% chance of encountering false positives or negatives in any given week. This occupancy sensor performance standard is listed by US Department of Energy in their Saving Energy Nationwide in Structures with Occupancy Recognition (SENSOR) Program overview [14].

In the presented work, we investigate the use of a PF for the purpose of estimating the human occupancy in an indoor environment while utilizing a minimal number of low-cost SLEEPIR sensor nodes. This effort aims to make the following key contributions. (1) We realize a particle filter based occupancy detection method that can achieve superior or equivalent accuracy when compared to statistical machine learning models. (2) Robust occupancy detection is achieved while maintaining a limited the sensor footprint in the monitored area. (3) The solution is scalable to variations in the room size, geometry, and overall monitored area size.

We present a literature review in section 2 that outlines the state-of-the-art in estimation methods for human occupancy detection. In section 3, we give a detailed description of the method along with a brief overview of the SLEEPIR sensor system that our method uses for occupancy estimation. Section 4 presents a brief discussion on the method

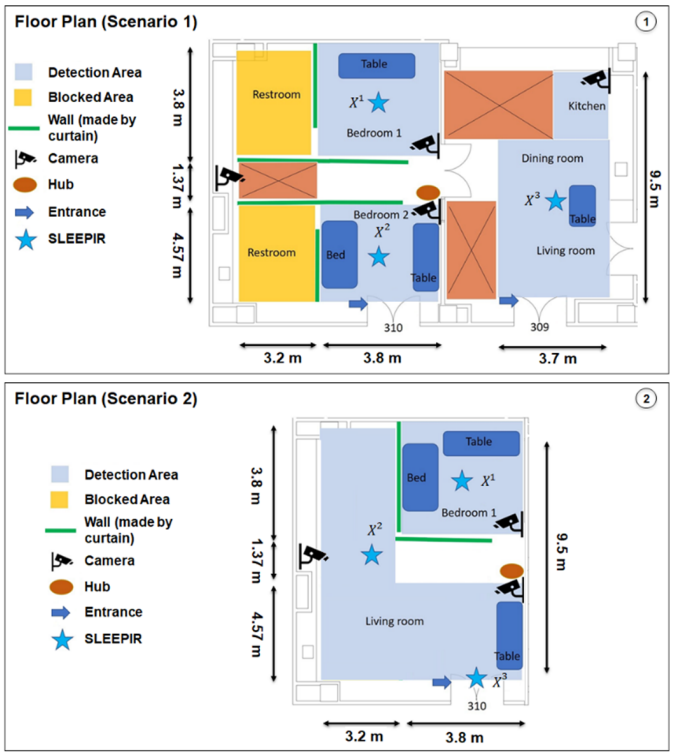


Fig. 1. We use two different floorplans as testbeds. We only use 3 SLEEPIR sensor nodes for each floorplan for dataset collection. Human occupancy is estimated for the locations $X^1$ through $X^3$. Ground truth is collected via surveillance cams.

and expected impact various parameters on system accuracy. Section 5 introduces dataset collection strategy and method performance evaluation. Section 6 gives a brief conclusion of the presented work.

## II. Literature Review

As such, there exists wide support in the literature for the fact that particle filters can be applied to complex systems through calculating a distribution of particles. PF accuracy can approach optimal estimation as it does not require the process and observation noise to have Gaussian distribution which is a requirement for traditional Gaussian filtering algorithms such as the Extended Kalman Filter (EKF) or Unscented Kalman Filter (UKF) [15]. Particle filters can estimate the actual state within a specific error range due to particles' dispersion that encompasses the possible hypothetical states in which the system can be. However, particle filters are challenging to optimally implement as these require a significantly large number of particles to produce accurate output and thus the calculation amount is much higher than that with the Gaussian approximation methods like EKF [16], which restricts their use in real-time application to some extent. To this end, a real-time EKF based networked sensor based occupancy estimation algorithm is proposed in [17]. This system estimates the number of occupants in each room of the monitored building. We have modified the proposed system to estimate the binary occupancy and have used its output to compare to our proposed PF output. The EKF system in [17] handles the non-linearity in the occupancy detection data by placing certain constraints on the model

e.g. placing upper bounds and lower bounds on exit/entrance rates, placing upper bounds on occupant flow from one room to another, conservation on the number of people in the building. We, on the other hand, use the PF to avoid making any such assumptions about occupant flow. Moreover, indoor occupancy over time is inherently a non-Gaussian estimation problem which cannot be optimally modelled via a filter that is based on Gaussian assumptions [18], hence a PF is the solution of choice for handling the non-Gaussian nature of the problem.

Among the Machine Learning (ML) based human tracking systems, there exists literature such as [10] where machine learning models are used to estimate human presence via PIR sensors. However, several drawbacks exist for any machine learning model to be able to perform optimally for human presence monitoring. Such methods require the pre-requisite of ground truth collection that is expensive and cannot be done with high certainty in many cases. Real-time performance is also hard to achieve in case online learning is desired for such systems. Typically for such real-time performance, high volume data-collection mechanisms along with high-end computational capability need to be available onboard the sensor nodes.

There are several other works that attempt to address the human tracking problem using PIR sensors. For example, in [19], binary sensed data obtained via PIR sensors attached to the ceiling of a room is used to estimate multiple human movement paths without a priori knowledge of the number of humans in the room. This method cannot address the PIR sensor's weakness i.e., sensor triggers regardless of whether it detects one or multiple people. Thus, although the method dynamically estimates human positions using the weighted centers of grouped fired infrared sensors, there is high uncertainty involved when large number of human subjects present in the observed area. Some relatively simple algorithms such as [20] use PIR sensors to record past occupancy patterns and then given a partially observed current day, the algorithm finds the five best matches in the past. The algorithm then averages the remainder of those matched days to compute probabilities for future occupancy.

Another work which takes an approach like ours is presented in [21], presents a case study of applying particle filters to location estimation for ubiquitous computing. This work uses two different sensors i.e., PIR and ultrasonic sensors, and fuses their output to establish human tracking. This approach focuses on tracking individual location of human subjects through a human motion model and static sensor models. Our approach is more occupancy centric and does not cater for individual human subject locations. Moreover, our sensor model is dynamic and are based upon the continuously updated correlation matrix between multiple sensors present in the system. Another work presented in [22] uses the adjacency relationships between sensor nodes and the exact positions of the sensors are irrelevant. Here, the state of the system is modeled via Hidden Markov Model and off-the-shelf PIR sensors are used to collect observations. This model provides an accuracy up to 89% but requires placement of many sensors with minimal gaps in the coverage area.

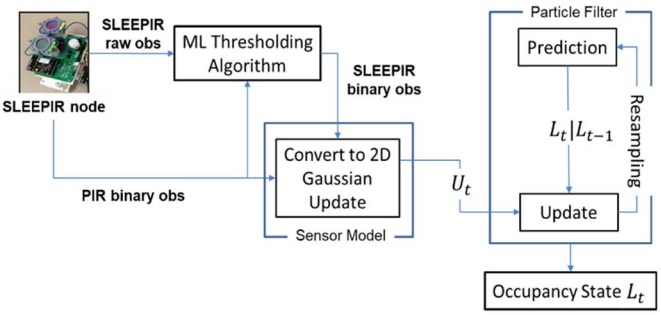


Fig. 2. PF based human occupancy detection method flow chart. Networked sensor nodes generate voltage, ambient temperature, and PIR data. The voltage is converted to binary occupancy observations via a thresholding algorithm. The node-level occupancy observations then update a system-level occupancy estimate via a PF.

## III. System Input and Pre-Processing Algorithms

The overall system flowchart is presented in figure 2. The raw SLEEPIR sensor observations are extracted from the SLEEPIR sensor using a Bluetooth communication protocol. The sensor and communication platform details are presented in section 3. A. We present a brief overall algorithm flow below that summarizes the flowchart presented in figure 2.

1. The raw sensor inputs which include SLEEPIR sensor voltage, PIR sensor binary output and ambient temperature are collected from each sensor node via a Bluetooth communication protocol.
2. Raw voltage values from SLEEPIR sensor are pre-processed using a machine learning based thresholding algorithm. This algorithm is detailed in section 3.B. The thresholding algorithm interprets the raw SLEEPIR sensor observations and outputs in binary whether the sensor has detected human occupancy or not. The traditional PIR sensor output is already binary, so it does not require preprocessing.
3. Since the binarized observations need to update a PF, we design a sensor likelihood model to shape an update for the PF. This sensor likelihood model merges the output from both the SLEEPIR sensor and the traditional PIR sensor into a single PF update. This model is described in detail in section 4.A.
4. The PF receives these periodic updates from the likelihood function and estimates the probability of human occupancy at each of the locations represented in the PF state. The world constraints are embedded in the likelihood and PF design thus the false positive or false negative observations get filtered and a robust human occupancy belief is estimated by the PF. Details of the PF sensor model, state update and prediction are presented in sections 4.B through 4.E.

### A. Synergistic SLEEPIR Sensor Module

The SLEEPIR sensor utilizes a LC shutter [23] and can significantly reduce the power consumption, weight, volume, and noise level, compared to other sensors that use mechanical choppers [1], [23], [24] for the purpose of stationary human

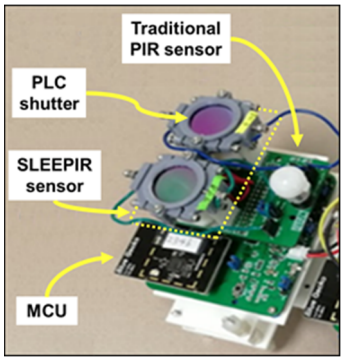


Fig. 3. SLEEPIR sensor node.

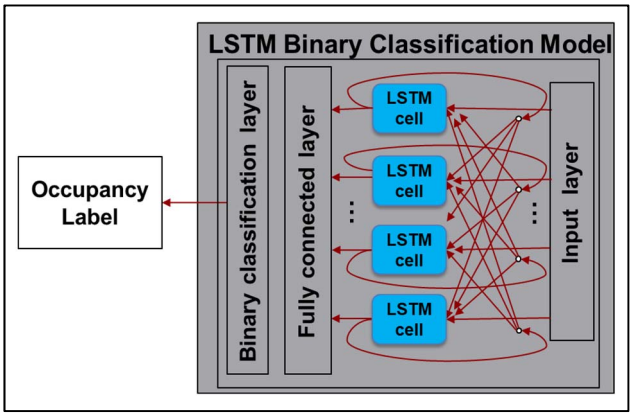


Fig. 4. LSTM network architecture for SLEEPIR raw observation binary classifier.

detection. The synergistic sensor module includes a SLEEPIR sensor alongside a traditional PIR sensor (EKMB1391111K, Panasonic Inc), a Microcontroller Unit (EFR32BG13, Silicon Labs), a driving circuit and two AA batteries connected in serials (3V DC voltage supply). The field of view (FOV) of the SLEEPIR and the PIR are 100(horizontal)×100(vertical) and 110(horizontal) 93(vertical) degrees, respectively. The maximum effective range of the sensor to detect stationary occupants is 3 m. The SLEEPIR sensor includes a LC shutter, and a PIR sensor without the Fresnel lens. SLEEPIR sensor is different from traditional PIR sensor in sense that the traditional PIR sensor has a Fresnel lens while the SLEEPIR does not. SLEEPIR's lab-made LC shutter consists of a high birefringence LC mixture, LCM-1660 (LC Matter Inc., USA), sandwiched by two Germanium windows, each with an anti-reflection (AR) coating on one side. Several other design parameters for this sensor are provided in [10]. The microcontroller unit (MCU) reads the analog signals from both the SLEEPIR and the PIR sensors via analog-digital converter (ADC) at a sampling frequency of 20Hz. After the MCU collects the sensing signals, it sends out the observations to the hub (Raspberry Pi) through a Bluetooth module for hard-drive storage.

As shown in Fig 3., as part of the SLEEPIR sensor, a pyroelectric sensing element, which is made up of pyroelectric material, converts the change of heat flux to current. If the radiation power received by the pyroelectric material is $W(t) = W_0 e^{i\omega t}$, which is modulated at frequency $\omega$, then voltage response $V_{out}(t)$ for the preamplifier stage is in the following form.

$$V_{out}(t) = \frac{R_{fb}\eta p' A\omega}{G_T\left(1+\omega^2\tau_T^2\right)^{\frac{1}{2}}\left(1+\omega^2\tau_E^2\right)^{\frac{1}{2}}} W(t) \qquad (1)$$

Here, $p'$ is the perpendicular component of the pyroelectric coefficient $p$. A is the area of the sensing element. $\eta$ represents the emissivity of sensing element; $\tau_T = H/G_T$ and $\tau_E = R_{fb}C_{fb}$ represent the thermal and electrical constant, respectively. Here $H, G_T, R_{fb}$ and $C_{fb}$ stand for thermal capacity, thermal conductance, feedback resistance, and capacitance, respectively. Commercial-of-the-shelf PIR sensors usually consist of two or four sensing elements placed in series with opposite polarizations. By covering the sensing elements with the same polarization, the transmission change of the LC shutter would introduce noticeable voltage signals from the PIR sensor. When the LC shutter, which is in front of the PIR sensor, changes its transmission periodically, the received radiation $W(t)$ changes periodically as well. This in turn causes the change of the output voltage $V_{out}(t)$.

### B. Machine Learning Based Thresholding Algorithm

Since sensor node generates time-series observations consisting of SLEEPIR raw voltage output $V_{out}(t)$ (see section 3.A), Ambient temperature $T_{amb}(t)$ and off-the-shelf PIR sensor output $PIR(t)$, we employ Recurrent Neural Networks (RNNs) to classify whether the observation indicate human occupancy or not. Recurrent neural networks (RNNs), in comparison to the typical feedforward neural networks (FFNNs), have been shown to achieve the highest accuracy with time-series data [25], as they can process and encode the sequential temporal information contained in a time-series data. First, the incoming time-series data from the sensor node is zero-centered and normalized. We then perform input quantization step. Reason for choosing to quantize input data is given in upcoming sub-section. We then divide the input time-series into pre-determined sized observation windows. Each window is then labeled as either occupied or unoccupied based on the available ground-truth gathered via web-camera installed testbed. Lastly, we train a Long Short-Term Memory (LSTM) Network with the training data. We deploy the trained network (shown in figure 4) so that the network can distinguish between the observations indicating occupancy versus those indicating non-occupancy. We detail the thresholding algorithm in the following sub-sections.

*1) Input Formatting and Quantization:* The goal of hand-tuned machine learning features used widely in the literature, is to produce easily distinguishable values for various data classes. A good feature remains invariant to the slight changes in the input pattern for a particular class and tends to produce roughly similar values for patterns belonging to the same class. We achieve the same effect by quantizing the input signal so that input signals that bear slight differences with each other, are quantized into similar looking patterns. Input quantization has a proven positive impact on RNN accuracy [26]. So, we choose

a quantization strategy that quantizes the sensor data to three levels (rise/fall/no change). It may be noted that the quantization used here is applied to both the training and test data streams. Equation 2 outlines the quantization function for the incoming observation at time t.

$$\begin{aligned} &if\ obs_t > obs_{t+1} + \epsilon \quad 1\,(rise) \\ &if\ obs_t < obs_{t+1} - \epsilon \quad -1\,(fall) \\ &if\ abs(obs_{t+1} - obs_t) \leq \epsilon \quad 0\,(no\ change) \end{aligned} \tag{2}$$

Literature suggests that a reasonable value for $\epsilon$ can be $(\mu_a + \sigma_a/2)$ [27], where $\mu_a$ and $\sigma_a$ are the mean and variance for the input distribution. Thus, the value of $\epsilon$ depends upon the distribution of observation elements $[V_{pp1}(t), V_{pp2}(t), T_{amb}(t), PIR(t)]$.

*2) Sliding Window Input Approach:* We initialize the training dataset $obs_T$ where each element is created by sliding a fixed-horizon window of length $l$ over the 4-D training input time-series consisting of following elements $[V_{pp1}(t), V_{pp2}(t), T_{amb}(t), PIR(t)]$. We then initialize the labels $label_T$ where each element corresponds to each window in $obs_T$. We set an element to "*occupied*" if a surveillance camera-based *ground-truth*$_T$ indicates that human subject was present for more than 50% of observations in the FOV of the sensor. Otherwise, the element is set to "*unoccupied*". A suitable window length ($l$) is found to be a critical parameter that has a pronounced impact on the over network accuracy. We will highlight this impact in the sub-section 3.B-4.

*3) RNN Network Architecture:* We use the well-cited deep forward RNN model proposed in [28], which contains multiple layers of recurrent units that are connected "forward" in time. The model architecture is simple yet powerful enough to produce reliable results over publicly available datasets which consist of time-series data. The online LSTM model shown in the figure 4 contains a single hidden layer of 16 recurrent neurons. During the evaluation phase, all RNN models use 3, 6, 9 and 16 neurons depending upon the experiment configuration. There are also 4 input neurons to match the number of input time-series from the sensor node i.e., $[V_{pp1}(t), V_{pp2}(t), T_{amb}(t), PIR(t)]$. There are two output neurons to match the output classes corresponding to "occupied" and "unoccupied" status.

*4) Performance Evaluation of LSTM and Other RNNs:* We performed a comprehensive search for a suitable RNNs. Our analysis included testing the collected dataset over LSTM, Bi-directional LSTM, Continuous-Time Recurrent Neural Network (CTRNN), Minimal Gated Unit (MGU) [20] and Gated Recurrent Unit (GRU) networks. We also varied the observation window length $l$ over a reasonable range to see if certain networks perform better than others. We found that for $l = 60$ *sec*, the accuracy was highest across all architectures. This indicates that the most effective discriminating features exist over a period of 60 seconds. It is important to mention here that SLEEPIR collects two consecutive observations over a span of 60 seconds. Moreover, we also vary the number of nodes for each network to see the impact of network size over accuracy. We varied the network size to improve classifier efficiency as the classifier is expected to perform in an online pipeline (refer to figure 2 to see pipeline). Table I and figure 5 outlines the performance evaluation results for RNN classifiers. We observe that LSTM and Bi-LSTM outperformed other RNNs in nearly all configurations. We selected LSTM as our network of choice as it is relatively less expensive in terms of resources. We encountered a relatively high ratio of false negatives compared to false positives. Reasons for this are discussed in section 4.

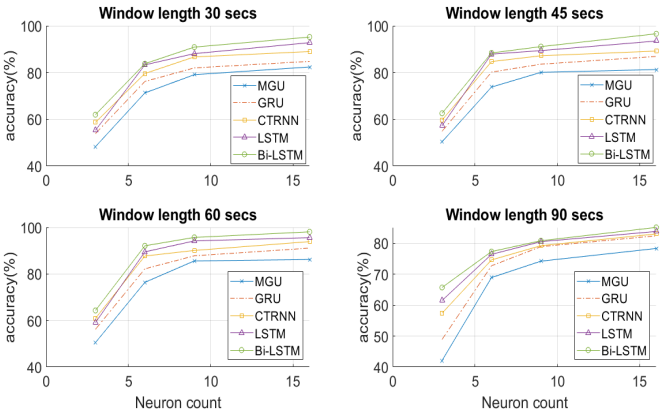


Fig. 5. Accuracy comparison between different RNNs with varying network size and observation window length *l*.

TABLE I
IMPACT OF OBSERVATION WINDOW SIZE AND NETWORK ARCHITECTURE ON ACCURACY

| Observation Window length | Average accuracy for 16 neurons hidden layer model. (50% labeling threshold) Quantized Observations | | | | |
|---|---|---|---|---|---|
| | Bi-LSTM | LSTM | CTRNN | GRU | MGU |
| 30 sec | 95.2% | 92.8% | 89.0% | 84.8% | 82.4% |
| 45 sec | 96.6% | 93.5% | 89.2% | 86.9% | 81.3% |
| 60 sec | 98.1% | 95.6% | 93.9% | 91.1% | 86.2% |
| 90 sec | 85.1% | 83.8% | 83.0% | 82.4% | 78.3% |

## IV. PARTICLE FILTER DESIGN

After the system observations are binarized via the proposed ML architecture, these observations are used to update a PF. The elements of this filter that include likelihood model, filter state, update and sampling modules, are detailed in the remaining of this section.

### A. Sensor Likelihood Model

We create a likelihood model based on the sensor coverage parameters and inter-sensor correlation measure. An observation from a sensor node that includes a SLEEPIR and PIR sensor, has a distribution of detection probabilities associated to the area that the sensor observes. This distribution of detection probability is based on SLEEPIR sensor range and field-of-view (FoV) experiments conducted in our earlier works [10], [11]. These works also discuss in detail the sensor installation height and orientation choices. Both FoV and range of the sensor are listed in section 3.A. Moreover, as a result of experimentation in [10], more specifically, we found that

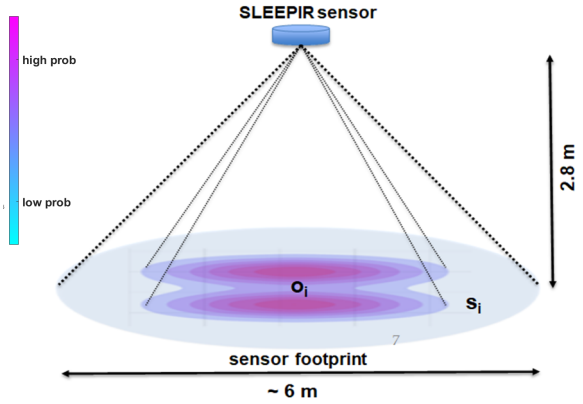


Fig. 6. SLEEPIR and PIR sensor multimodal detection probability distribution is shown. The distribution works as a measurement update for the SLEEPIR and PIR sensors. $\boldsymbol{o_i}$ is the sensor footprint ($\sim \mathbf{4m^2}$) for the SLEEPIR sensor while $\boldsymbol{s_i}$ is the sensor footprint (($\sim \mathbf{18m^2}$) for the PIR sensor.

for sensor installed at a height of 2.8 meters, the radius of SLEEPIR footprint is 1.2 meters while the radius of concentric PIR sensor footprint is 2.4 meters. These footprints are visually represented in figure 6 where a sensor cone is also shown. Each sensor generates a timestamped log of occupancy status observations as follows.

$$\begin{aligned} D_t^{iSLEEPIR} &= \left\{(i,t) : i \epsilon N, t \epsilon \mathbb{R}^+\right\} \\ D_t^{iPIR} &= \left\{(i,t) : i \epsilon N, t \epsilon \mathbb{R}^+\right\} \end{aligned} \tag{3}$$

In the equation (3) $(i,t)$ denotes that sensor i triggers at time t. Figure 1 shows the set of locations denoted by index $i$ i.e., $X^1, X^2, X^3$. Whenever an occupancy $D_t^i$ observation indicates a human detection, we adjust the variance for bivariate Gaussian update in the following way.

$$\begin{aligned} \sigma_t^{\upsilon SLEEPIR} &= \frac{1}{\rho_{i\upsilon}} \times \sigma_t^{\upsilon SLEEPIR} \\ \sigma_t^{\upsilon PIR} &= \frac{1}{\gamma_{i\upsilon}} \times \sigma_t^{\upsilon PIR} \end{aligned} \tag{4}$$

Here matrices $\gamma$ and $\rho$ represent the Pearson-correlation coefficient between smoothed sensor observations $D_t^{iPIR}$ and $D_t^{iSLEEPIR}$ respectively. For example, $\rho_{ii}$, would represent the sensor observation correlation with itself which will always be 1. In case sensor $i$ is not correlated with sensor $\upsilon$, $\rho_{i\upsilon}$ will be near the value of 0. In other words, the inter-sensor correlation matrices ensure that if sensor $i$ triggers and it happens to have its observations correlated to sensor $\upsilon$, the sensor model will indicate the sensor $\upsilon$ as a triggering sensor as well albeit with a reduced amount of certainty. This amount depends upon the level of correlation present between two sensors. It must be noted that we smooth the observations by a certain time-window $\tau$ Thus, the correlation represented in $\gamma$ and $\rho$ is a correlation over a time-window $\tau$.

The mean $\mu^i$ for update distribution for sensor $i$, is set to the 2D sensor coordinates in the map while unadjusted variance $\sigma^i$ is set according to the following evaluation functions.

$$\sigma_t^{iSLEEPIR} \propto \left(\frac{o_i}{s_i + l_i}\right), \quad \sigma_t^{iPIR} \propto \left(\frac{o_i + s_i}{l_i}\right) \tag{5}$$

We then define $bivariateGaussianGen$ function so we can generate a single mode bivariate gaussian distribution for PIR sensor. We define $mmBivariateGaussianGen$ function to generate the bimodal Gaussian distribution for SLEEPIR sensor. Both distributions are shown in figure 6 and function definitions are listed in equation 6.

$$\begin{aligned} \pi^{iPIR} &= bivariateGaussianGen\left(\mu^i, \sigma^{iPIR}\right) \\ \pi^{iSLEEPIR1} &= mmBivariateGaussianGen \\ &\quad \times \left(\mu^i, \sigma^{iSLEEPIR}\right) \end{aligned} \tag{6}$$

The variance of these gaussian distributions depend upon the size of areas falling under each of their observation cones. Thus, $\sigma_t^{iSLEEPIR}$ and $\sigma_t^{iPIR}$ represent the uncertainity for measurement update distributions $\pi^{iPIR}$ and $\pi^{iSLEEPIR}$. $\sigma_t^{iSLEEPIR}$ and $\sigma_t^{iPIR}$ are directly proportional to the ratio of area observed by the sensors to the total area of the room the sensor is installed in.

### B. Particle Filter State

The goal of the filter is to estimate the occupancy of the observed area with a level of certainty. We choose to represent the occupancy belief over the expanse of observed space via a multimodal Gaussian bivariate distribution represented by $L_t$. Variable $L_t$ is defined as

$$\begin{aligned} L_t &= \left\{\pi_t^{u\upsilon}\right\} \\ where, \quad u &= -lim_x + r, -lim_x + 2r, \ldots, lim_x \\ and\ \upsilon &= -lim_y + r, -lim_y + 2r, \ldots, lim_y \end{aligned}$$

Here $u$ $and$ $\upsilon$ are indexes that run through the range of weights $\pi$ which is a bivariate probability density function (pdf) that represents the bivariate probability distribution indicating the occupancy probability across the 2D spatial expanse of area under monitoring. The area dimensions are $2lim_x \times 2lim_y$. Here changing the value of $r$ (or resolution) changes the size of domain of the distribution function. We found empirically that an optimal value for $r$ is 0.5 meters. The value of $r$ can impact the accuracy and execution efficiency of the PF.

Each particle in the filter contains a varying multimodal bivariate Gaussian distribution for the area under observation. We initialize $Q$ particles under certain initial conditions.

$$P_t^j = initialize\left(L_t^j\right) \quad where \quad j = 1, \ldots, Q \tag{7}$$

Each particle is initialized by adding normal random noise to an initial hypothetical update $U_0$ where no sensor is triggered. The update $U$ is the based on augmented sensor signals received from all sensors in the system i.e., $X^1, X^2 or X^3$. We use index $j$ as a particle index invariably for the remaining article.

### C. Prediction Step

We know that the PF involves repetitive prediction and update steps. In the prediction step, we first generate a uniformly distributed random number $h \in [0, 1]$ and then use it to select sample $P_{t-1}^j$ from all samples at time $t-1$ according

to their weights $w_t^i$. Then the prediction step is performed for each $P_t^j$ as follows

$$L_{t+1}^j = L_t^j + n_{spread}$$

Here $n_s$ is a multimodal normally distributed random noise that has modes centered at sensor locations $\mu^i$. Essentially $n_s$ factors in the variation present in the rate at which human subjects move their positions from sensor to sensor within the monitored area.

### D. Update Step

For each particle $P_t^j$, following steps update the particle variable $L_t^j$ at each time-step via a Gaussian update $U_t$ via the following expression.

$$L_{t+1}^j = L_t^j + \delta_{t+1}(U_{t+1}^i - L_t^j) \tag{8}$$

Here,

$$U_t = \left\{\pi_t^{uv}\right\}$$

Variance $\sigma_t^i$ for $U_t$ is already defined earlier in the section 3.B. $u$ and $v$ have already been defined in while defining the PF state. Moreover,

$$\delta_{t+1} = \frac{\sigma_t^2}{\sigma_t^2 + \sigma_{t+1}^2} \tag{9}$$

Here if $U_{t+1}^i$ has high variance relative to $U_t^i$ then $\delta_{t+1}$ is small thus it has little impact on value of $L_{t+1}^j$. This ensures that updates which have more chance of error are factored-in less into our current belief $L_{t+1}^j$.

### E. Sampling Step

In the sampling step, we set weight for each particle and then perform a weighted sampling to select particles for prediction step. Weights for particles are set higher that have smaller Bhattacharya distance [29] (measures the similarity between two distributions). Since each particle, $P_t^j$ is comprised of bivariate distribution $L_t^j$, we evaluate the bivariate Bhattacharya distance between the update $U_t$ and each particle $L_t^j$. Following step presents the probability of a particle to be sampled via the Bhattacharya distance-based weights.

$$Prob^j\left(w_t^j \mid U_t\right) = \frac{1}{\sqrt{2\pi}\,\delta_t} = e^{-\frac{\left(Bhattayacharya\left(P_t^j - U_t\right)\right)^2}{2(\delta_t)^2}}$$

## V. Discussion

Sensor model-based updates are critical to the performance of the proposed filter. These updates if modelled correctly can optimally select and help propagate particles that are very close to the real-world occupancy scenario. It is thus useful to visualize and have a critical look at one example of sensor model-based update. We can see this bivariate gaussian update in figure 6. Since the sensors at locations $X^1$ and $X^2$ have correlated observations, the update factors-in this correlation and hypothesizes a more realistic update. We may highlight here that correlation evaluation can be erroneous in case there is infra-red (IR) noise present in the observed space. This noise can include electronic devices and objects that efficiently absorb the heat radiated by human body. We can also observe that particle sensor model heavily relies on certain parameters that are rooted in real world environmental factors and sensor limitations. A list of these tunable parameters is provided in table II. Any changes in these parameters can have a pronounced impact on PF accuracy.

TABLE II
Brief Description of Method Parameters

| Parameter | Explanation |
|---|---|
| $Vppr, Vppf$ thresholds | Both thresholds help us deal with the SLEEPIR sensor noise as detailed in [30] |
| $\rho_{uv}, \gamma_{uv}$ | Time-window based correlation coefficient for human detection between observation time-series collected at two locations. These helps us configure the sensor model. Details presented in section 4.A. |
| $\beta^i$ | This threshold is applied to the value of bivariate gaussian curve at its mean in $L_t^j$. If this value is beyond this threshold, human presence is established. |
| $\eta_t, \eta_{spread}$ | These gaussian noise parameters for the filter. $\eta_t$ is the noise present in the timestamps of the updates. $\eta_{spread}$ is the noise present in the velocity of human subjects. |

## VI. Results

### A. Dataset

We used a dataset that employs three SLEEPIR sensor nodes. We deployed the nodes in two configurations as shown in figure 1. Each node collects the observation every 30 seconds. The SLEEPIR observations $D_t^{iSLEEPIR}$ were evaluated using the raw SLEEPIR sensor voltage values. Certain thresholds were used to remove noisy observations as per the literature presented in [10]. Surveillance cameras were used to label the ground-truth. Data for a total of 15 days was collected. We used 7 days to extract correlation matrices $\gamma$ and $\rho$ for sensors. It may be noted here that distinct correlation matrices were extracted for each of the floorplan scenario presented in figure 1. The observation correlation between sensor pairs within a scenario plays a crucial role in the performance of particle filter-based occupancy detection. We observed that the Peterson's correlation coefficient evaluated over a longer period was higher and thus produced better results. Figure 8 illustrates the relationship between the observation timespan and evaluated correlation for a particular sensor pair. After using 7 days of data to extract correlation matrices, we used the remaining 8 days of test data for evaluation. We down sampled the observations to 1 observation per minute. This provided us with a total of 21600 observations within the dataset. A total of 4 subjects (2 males and 2 females) were employed to gather the dataset.

### B. Accuracy Results

This work claims to minimize the sensor footprint and deliver comparable human presence accuracy when compared to statistical ML methods. We also studied the impact of the number of sensors on the occupancy detection accuracy and found that 3 sensor nodes suffice the 95% true positive

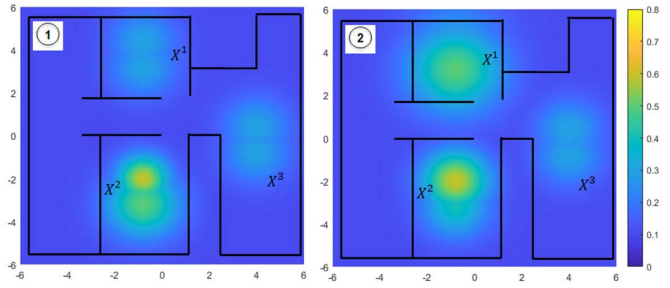


Fig. 7. Inset label 1 shows the bivariate multimodal distribution for the update produced by the sensor model when the subject is near sensor $X^2$. Inset label 2 shows the gaussian profile for the update when the subject leaves the vicinity of sensor $X^2$ and approaches sensor $X^1$. Both x and y axis are labeled in meters.

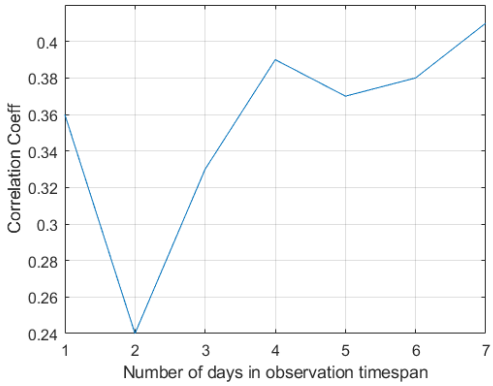


Fig. 8. Peterson's correlation coefficient for the sensor pair $X^1$ and $X^2$ in scenario 2, is shown to increase as the timespan for observations is increased from 1 day to 7 days.

TABLE III
IMPACT OF REDUCTION OF SENSOR NODES IN THE NETWORK

| Date | Scenario | 1-Sensor Accuracy ($X^3$) (%) | 2-Sensor Accuracy ($X^2, X^3$) (%) | 3-Sensor Accuracy ($X^1, X^2, X^3$) (%) |
|---|---|---|---|---|
| 25-Feb | 1 | 27.73 | 76.91 | 98.83 |
| 26-Feb | 1 | 24.04 | 75.11 | 94.21 |
| 1-Mar | 1 | 19.60 | 77.87 | 95.70 |
| 2-Mar | 1 | 22.64 | 67.25 | 93.37 |
| 6-Mar | 1 | 20.01 | 79.88 | 95.69 |
| 20-Oct | 2 | 46.49 | 88.53 | 96.55 |
| 3-Nov | 2 | 53.91 | 81.03 | 97.34 |
| 4-Nov | 2 | 58.27 | 85.35 | 98.10 |

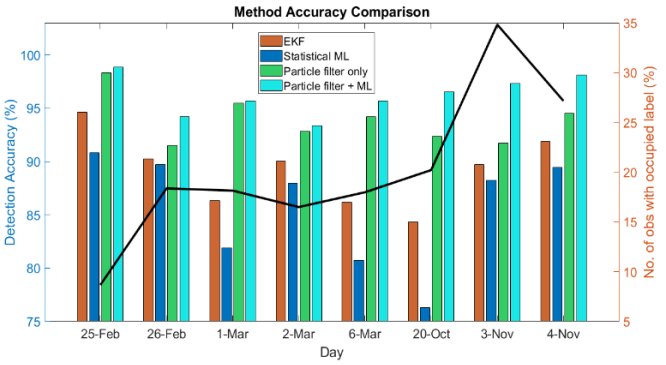


Fig. 9. Accuracy comparison with baseline Statistical Machine Learning Model. Accuracy improvement due to PF (green) and added improvement via adding ML in the pipeline (light blue) is shown. The line graph shows the percentage of occupied observations in the test-dataset.

TABLE IV
ACCURACY COMPARISON BETWEEN BASELINE AND PROPOSED MODELS

| Date | Scenario | EKF | | Statistical ML (%) | PF only (%) | | PF with ML (%) |
|---|---|---|---|---|---|---|---|
| | | acc (%) | avg exec time (ms) | | acc (%) | avg exec time (ms) | |
| 25-Feb | 1 | 94.61 | 88 | 90.82 | 98.35 | 461 | 98.83 |
| 26-Feb | 1 | 90.24 | 86 | 89.71 | 91.51 | 738 | 94.21 |
| 1-Mar | 1 | 86.35 | 87 | 81.91 | 95.47 | 693 | 95.70 |
| 2-Mar | 1 | 90.02 | 89 | 87.96 | 92.83 | 727 | 93.37 |
| 6-Mar | 1 | 86.15 | 88 | 80.73 | 94.22 | 824 | 95.69 |
| 20-Oct | 2 | 84.33 | 86 | 76.27 | 92.36 | 720 | 96.55 |
| 3-Nov | 2 | 89.70 | 87 | 88.25 | 91.72 | 602 | 97.34 |
| 4-Nov | 2 | 91.86 | 87 | 89.46 | 94.51 | 415 | 98.10 |


Fig. 10. (Left) Mattress still emitting IR after 60 seconds have passed since the subject left the bed. (Right) Top view of a chair, a laptop, and a charger. Chair seat is still radiating IR after the human subject has left. All IR sources mentioned here emit IR noise for a machine learning based classifier.

accuracy criteria mentioned in the US Department of Energy SENSOR program outline [14]. The results of this comparative experiment are listed in table III.

It may be mentioned here that we used the proposed system-level PF algorithm for the experiment results shown in table III. As a consequence of this experiment, we employed observations from 3 nodes (3 PIR and 3 SLEEPIR sensors) to compare the accuracy between sensor-level algorithm (Statistical ML) [10] and the system-level algorithms (EKF [19], PF and proposed PF with ML algorithms). Sensor-level machine learning based occupancy detection algorithm results presented in [10] are used as a baseline for our analysis. We applied the EKF based networked sensor estimation algorithm given in [17], to our dataset and got inferior accuracy results compared to our proposed PF algorithm. Not only, we do an accuracy comparison between EKF and PF approach, we also highlight the performance penalty of choosing to prefer PF over EKF to achieve higher accuracy. Table IV shows the average processing time for a single observation of window length 60 secs. The execution times were measured on a Raspberry Pi 4 using a 64-quad-core Cortex-A72 (ARM v8) processor. We choose not to involve the Machine learning layers in the performance comparison as the computation cost for the ML inference

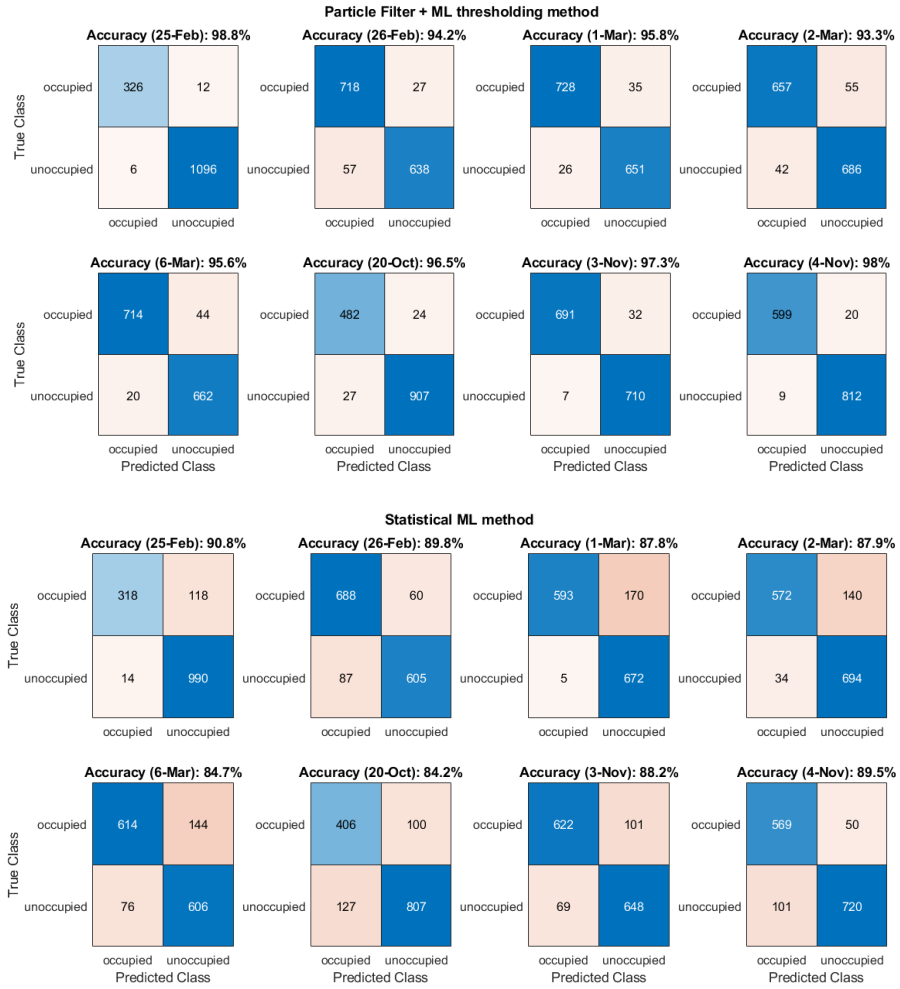


Fig. 11. Confusion matrices showing the performance comparison between the state-of-the-art Statistical ML occupancy detection method and the proposed method. The occupancy ground truth was collected via surveillance cameras.

is negligible. We have been able to show (See figure 9) that the proposed Particle Filtering approach is able to provide superior accuracy when compared to accuracy achieved via an ML based statistical thresholding approach [10] and a system-level EKF based occupancy estimation algorithm [31].

When compared to [10], we were also able to reduce the number of sensors that are required to determine the occupancy in the indoor space. The last two columns of Table IV shows human occupancy accuracy via two input pre-processing approaches (a) The system-level human occupancy is established via a PF that uses a fixed threshold to convert incoming sensor voltage into binary inputs. Let us term this as "PF only" approach. (b) The system-level human occupancy is established via the proposed machine learning classifier that is described in section 3.B. Let us label this as "PF with ML thresholding" approach. For both these approaches, the system level-human occupancy is established if the PF output probability density function results in at least a single occupancy peak. Examples of such peaks are shown in figure 7 in elevated temperature color shades. Figure 9, via the line graph, also shows the percentage of observations in the test-dataset where at least one occupant was present in the observed area. We establish the presence of the occupant via ground truth data. This percentage is important as the system does not encounter significant detection errors whenever human subjects are not around. We also tested the proposed method using two test-bed scenarios (see figure 1). The first scenario tests the method performance in space that is very restrictive for the sensor's range and correlation between the sensors is low as each sensor is housed in an independent room. The second scenario has more open space available to the sensors and moreover two sensors although far from each other, are housed within a same enclosure i.e., a large living room.

### C. Results Discussion

Despite the robust performance at the system-level, delivered by the PF, false negatives remain a problem at the sensor-level. The IR noise present in the environment is mostly due to the heat transferred to the objects with which the human body gets in contact. These keep emitting IR radiation even after the human subject leaves the observed area. Moreover, the IR radiation emitted by certain bodies that have temperature and emissivity values similar to the human body, acts as noise whenever we attempt to train a classifier for occupancy decisions. Figure 10 shows examples of IR noise within our testbed that we were able to discover during the

experimentation. We were able to show false positives and false negatives for each day of the test dataset as shown in figure 11.

We must mention here that false positives generated due to objects that acquire human body temperature are transient as these objects cool down within minutes. As a future effort, we are developing an ML training algorithm that can discriminate between human body that maintains a near constant temperature and objects that are in the process of cooling down. It can be observed that the proposed method consistently produces more false negatives compared to false positives. This is obviously due to the IR noise present in the environment. It can also be seen that certain false positives are also produced. There are two primary contributors towards false negatives. Firstly, the IR radiated by certain subjects is simply not enough and due to small body size and clothing. Secondly, certain PF parameters may not be tuned well to suit the test-bed dynamics e.g., Gaussian noise parameters $\eta_t, \eta_{spread}$ may need to be hand-tuned to be sensitive to the speed with which human subject approaches and leaves the sensor vicinity. One of the possible solutions is adaptive PF parameter tuning but further analysis and investigation is necessary to propose a parameter tuning strategy. The accuracy results are highly reliant on the correlation measure between the observations from any two sensor nodes used for experimentation.

## VII. Conclusion

The proposed method delivers robust results in terms of human occupancy detection while using a small number of low-powered SLEEPIR and PIR sensors. The model exploits the inter-location observation correlation between sensors to generate close to the real-world measurement updates. Moreover, it exploits the temporal bounds on the position change rate of human subjects within the environment. The novel bivariate update distribution generated by the sensor model ensures that realistic and not random hypothesis (particles) are generated for the PF to sample from. Not only is this method comparable to the contemporary statistical ML method [10] but it also attempts to reduce the number of required sensors to deliver the same accuracy for human presence detection. The method is evaluated over two different testbeds with different sensor configurations. The consistent accuracy reveals the scalability of the proposed method. Moreover, the method's dependence over ground-truth to extract observation correlation between different sensors is dependent on the accuracy of ground-truth annotation. As a future effort, alternative methods can be explored to extract observation correlation between different locations.

## References


[1] L. Wu, Y. Wang, and H. Liu, "Occupancy detection and localization by monitoring nonlinear energy flow of a shuttered passive infrared sensor," *IEEE Sensors J.*, vol. 18, no. 21, pp. 8656–8666, Nov. 2018.

[2] S. Zhang, K. Liu, Y. Zhang, and Y. Wang, "A coarse fingerprint-assisted multiple target indoor device-free localization with visible light sensing," *IEEE Sensors J.*, vol. 22, no. 2, pp. 1461–1473, Nov. 2021, doi: 10.1109/JSEN.2021.3130711.

[3] L. Wu and Y. Wang, "Compressive sensing based indoor occupancy positioning using a single thermopile point detector with a coded binary mask," *IEEE Sensors Lett.*, vol. 3, no. 12, pp. 1–4, Dec. 2019, doi: 10.1109/LSENS.2019.2955125.

[4] Z. Chen and Y. Wang, "Infrared–ultrasonic sensor fusion for support vector machine–based fall detection," *J. Intell. Mater. Syst. Struct.*, vol. 29, no. 9, pp. 2027–2039, May 2018, doi: 10.1177/1045389X18758183.

[5] R. Hua and Y. Wang, "Monitoring insole (MONI): A low power solution toward daily gait monitoring and analysis," *IEEE Sensors J.*, vol. 19, no. 15, pp. 6410–6420, Apr. 2019, doi: 10.1109/JSEN.2019.2910105.

[6] Z. Chen and Y. Wang, "Remote recognition of in-bed postures using a thermopile array sensor with machine learning," *IEEE Sensors J.*, vol. 21, no. 9, pp. 10428–10436, May 2021, doi: 10.1109/JSEN.2021.3059681.

[7] Z. Chen, Y. Wang, and H. Liu, "Unobtrusive sensor-based occupancy facing direction detection and tracking using advanced machine learning algorithms," *IEEE Sensors J.*, vol. 18, no. 15, pp. 6360–6368, Aug. 2018, doi: 10.1109/JSEN.2018.2844252.

[8] J. Andrews, M. Kowsika, A. Vakil, and J. Li, "A motion induced passive infrared (PIR) sensor for stationary human occupancy detection," in *Proc. IEEE/ION Position, Location Navigat. Symp. (PLANS)*, Apr. 2020, pp. 1295–1304, doi: 10.1109/PLANS46316.2020.9109909.

[9] A. D. Shetty, D. B. Shubha, and K. Suryanarayana, "Detection and tracking of a human using the infrared thermopile array sensor—'Grid-EYE,"' in *Proc. Int. Conf. Intell. Comput., Instrum. Control Technol. (ICICICT)*, Jul. 2017, pp. 1490–1495, doi: 10.1109/ICICICT1.2017.8342790.

[10] L. Wu and Y. Wang, "Stationary and moving occupancy detection using the SLEEPIR sensor module and machine learning," *IEEE Sensors J.*, vol. 21, no. 13, pp. 14701–14708, Jul. 2021.

[11] L. Wu, F. Gou, S.-T. Wu, and Y. Wang, "SLEEPIR: Synchronized low-energy electronically chopped PIR sensor for true presence detection," *IEEE Sensors Lett.*, vol. 4, no. 3, pp. 1–4, Mar. 2020.

[12] L. Wu, Z. Chen, and Y. Wang, "Occupancy detection using a temperature-sensitive adaptive algorithm," *IEEE Sensors Lett.*, vol. 5, no. 12, pp. 1–10, Nov. 2021, doi: 10.1109/LSENS.2021.3126285.

[13] L. Wu and Y. Wang, "Performance optimization of the SLEEPIR sensor towards indoor stationary occupancy detection," *IEEE Sensors J.*, vol. 21, no. 21, pp. 23776–23786, Nov. 2021, doi: 10.1109/JSEN.2021.3111877.

[14] D. M. Sofos. (2022). *Saving Energy Nationwide in Structures With Occupancy Recognition*. [Online]. Available: https://arpa-e.energy.gov/?q=arpa-e-programs/sensor

[15] M. St-Pierre and D. Gingras, "Comparison between the unscented Kalman filter and the extended Kalman filter for the position estimation module of an integrated navigation information system," in *Proc. IEEE Intell. Veh. Symp.*, Jun. 2004, pp. 831–835, doi: 10.1109/IVS.2004.1336492.

[16] K. György, A. Kelemen, and L. Dávid, "Unscented Kalman filters and particle filter methods for nonlinear state estimation," *Proc. Technol.*, vol. 12, pp. 65–74, Jan. 2014, doi: 10.1016/j.protcy.2013.12.457.

[17] R. Tomastik, S. Narayanan, A. Banaszuk, and S. Meyn, "Model-based real-time estimation of building occupancy during emergency egress," in *Pedestrian and Evacuation Dynamics*. Berlin, Germany: Springer, 2010, pp. 215–224.

[18] M. S. Arulampalam, S. Maskell, N. Gordon, and T. Clapp, "A tutorial on particle filters for online nonlinear/non-Gaussian Bayesian tracking," *IEEE Trans. Signal Process.*, vol. 50, no. 2, pp. 174–188, Feb. 2002, doi: 10.1109/78.978374.

[19] T. Miyazaki and Y. Kasama, "Multiple human tracking using binary infrared sensors," *Sensors*, vol. 15, no. 6, pp. 13459–13476, Jun. 2015.

[20] J. Scott *et al.*, "PreHeat: Controlling home heating using occupancy prediction," in *Proc. 13th Int. Conf. Ubiquitous Comput. (UbiComp)*, Sep. 2011, pp. 281–290.

[21] J. Hightower and G. Borriello, "PFs for location estimation in ubiquitous computing: A case study," in *Proc. Int. Conf. Ubiquitous Comput.* Berlin, Germany: Springer, 2004, pp. 88–106.

[22] H. Pulkkinen, "Improving energy efficiency with occupant tracking," M.S. thesis, Dept. Appl. Sci., Aalto Univ., 2016.

[23] L. Wu and Y. Wang, "A low-power electric-mechanical driving approach for true occupancy detection using a shuttered passive infrared sensor," *IEEE Sensors J.*, vol. 19, no. 1, pp. 47–57, Oct. 2018.

[24] H. Liu, Y. Wang, K. Wang, and H. Lin, "Turning a pyroelectric infrared motion sensor into a high-accuracy presence detector by using a narrow semi-transparent chopper," *Appl. Phys. Lett.*, vol. 111, no. 24, Dec. 2017, Art. no. 243901.

[25] Z. C. Lipton, J. Berkowitz, and C. Elkan, "A critical review of recurrent neural networks for sequence learning," 2015, *arXiv:1506.00019*.
[26] J. Suto, S. Oniga, and P. P. Sitar, "Feature analysis to human activity recognition," *Int. J. Comput. Commun. Control*, vol. 12, no. 1, pp. 116–130, Dec. 2016.
[27] M. Z. Alom, A. T. Moody, N. Maruyama, B. C. Van Essen, and T. M. Taha, "Effective quantization approaches for recurrent neural networks," in *Proc. Int. Joint Conf. Neural Netw. (IJCNN)*, Jul. 2018, pp. 1–8.
[28] N. Y. Hammerla, S. Halloran, and T. Ploetz, "Deep, convolutional, and recurrent models for human activity recognition using wearables," 2016, *arXiv:1604.08880*.
[29] A. Bhattacharyya, "On a measure of divergence between two statistical populations defined by their probability distributions," *Bull. Calcutta Math. Soc.*, vol. 35, no. 1, pp. 99–109, 1943.
[30] L. Wu and Y. Wang, "True presence detection via passive infrared sensor network using liquid crystal infrared shutters," in *Smart Materials, Adaptive Structures and Intelligent Systems*, vol. 84027. New York, NY, USA: American Society of Mechanical Engineers, 2020, Paper V001T08A004.
[31] J. Schiff and K. Goldberg, "Automated intruder tracking using particle filtering and a network of binary motion sensors," in *Proc. IEEE Int. Conf. Autom. Sci. Eng.*, Oct. 2006, pp. 580–587.

**Muhammad Emad-ud-Din** received the B.S. degree in software engineering from Foundation University, Pakistan, in 2004, and the M.S. degree in computer science from the University of Southern California in 2008. He is pursuing the Ph.D. degree in computer science with Texas A&M University. His research interests include machine learning, robotics, sensor modeling, and human activity recognition and tracking. He was a recipient of the Fulbright Scholarship.

**Zhangjie Chen** received the B.S. degree from Shanghai Jiao Tong University, Shanghai, China, in 2014, the M.S. degree in mechanical engineering from the University of Florida, FL, USA, in 2016, and the Ph.D. degree in mechanical engineering from Texas A&M University, College Station, TX, USA, in 2021. His research interests include occupancy sensing, activity recognition, control and actuation, and machine learning.

**Libo Wu** received the B.S. degree in applied physics from the University of Science and Technology of China, Hefei, Anhui, China, in 2015, and the Ph.D. degree in mechanical engineering from Texas A&M University, College Station, TX, USA, in 2021. His research interests include pyroelectrical sensors, thermopile sensors, and their applications for occupancy detection in indoor environment.

**Qijie Shen** received the B.S. degree in electronic engineering from Nanjing University, Nanjing, Jiangsu, China, in 2016, and the M.S. degree in computer engineering from Texas A&M University, College Station, TX, USA, in 2021. He is currently a Senior Engineer with Qualcomm Technologies, Inc., San Diego, CA, USA. His recent duties focus on 5G, DSP, and firmware development.

**Ya Wang** (Member, IEEE) received the B.S. degree in mechatronics from Shandong University, Jinan, Shandong, China, in 2004, the M.S. degree in mechanical engineering from the University of Puerto Rico, Mayagüez, PR, USA, in 2007, and the Ph.D. degree in mechanical engineering from the Virginia Polytechnic Institute and State University, Blacksburg, VA, USA, in 2012. She is currently an Associate Professor in Mechanical Engineering, Electrical and Computer Engineering, and Biomedical Engineering with Texas A&M University, College Station, TX, USA. She has authored one book chapter, 63 peer-reviewed journal papers, 40 conference proceeding papers, filed four U.S. utility patents, and two provisional patents. Her recent research interests include infrared sensing, signal processing, machine learning with applications in occupancy detection, human identification, and activity tracking.